

Supplementary Information

Highly Selective Ag Foam Gas Diffusion Electrodes for CO₂ Electroreduction by Pulsed Hydrogen Bubble Templatation

Hendrik Hoffmann^{1*}, Maximilian Kutter¹, Jens Osiewacz², Melanie-Cornelia Paulisch-Rinke³, Steffen Lechner¹, Barbara Ellendorff², Annika Hilgert¹, Ingo Manke³, Thomas Turek², and Christina Roth¹

¹Electrochemical Process Engineering, Universität Bayreuth, Universitätsstraße 30, 95447 Bayreuth, Germany.

²Institute of Chemical and Electrochemical Process Engineering, Clausthal University of Technology, Leibnizstrasse 17, 38678 Clausthal-Zellerfeld, Germany.

³Helmholtz-Zentrum Berlin für Materialien und Energie, Department Electrochemical Energy Storage, Hahn-Meitner-Platz 1, 14109 Berlin, Germany

*Corresponding author: hendrik.hoffmann@uni-bayreuth.de

Methods

Calculation of the Deposition Efficiency

The deposition efficiency of the Ag foam catalyst after Dynamic Hydrogen Bubble Templatation (DHBT) was calculated by equation (1), with n being the number of electrons being transferred during electrodeposition, F the Faraday constant, M_{Ag} the molar mass of Ag, I the deposition current and the deposition time t . The mass of the Ag catalysts before and after electrochemical deposition were calculated with respect to the total masses of the polymer substrates measured with a Kern ABT 220-5DM precision balance and a resolution of 0.01 mg. The samples were therefore dried in laboratory atmosphere at room temperature for 24 h.

$$\text{Deposition Efficiency}_{Ag} = \frac{m_{Ag}}{m_{theor.}} = \frac{m_{Ag} \cdot n \cdot F}{M_{Ag} \cdot I \cdot t} \quad (1)$$

Liquid product analysis

Liquid products were analyzed by NMR spectroscopy from the anolyte and catholyte solutions after 100 h of electrolysis. NMR measurements were performed on a Bruker Avance 300 spectrometer. The solvent residual peak of DMSO-*d*6 (2.50 ppm) was taken as an internal standard for the ¹H-NMR spectra. The ¹⁹F-NMR spectra were referenced to trichlorofluoromethane (CFCl₃) as external standard. The evaluation of the spectra was done using MestReNova software version 10.0.2.

DHBT process in galvanostatic mode

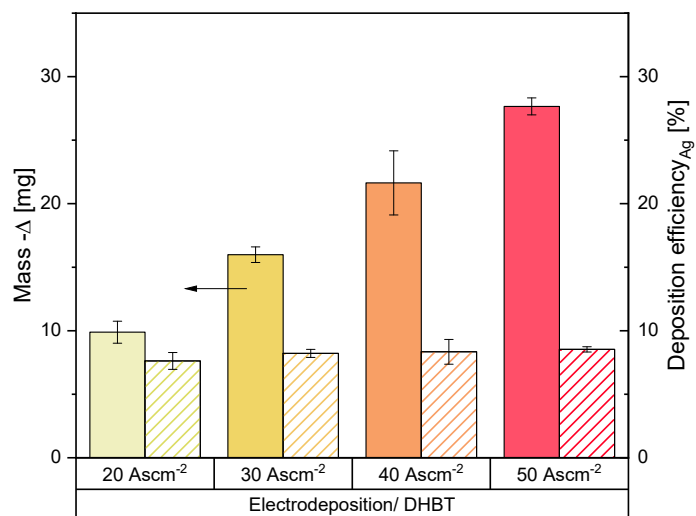


Figure 1: Deposited Ag mass and calculated Ag deposition efficiency of the DHBT foam electrodes with increasing charge densities during DC mode.

Electrochemical cell, used for CO_2RR of the Ag DHBT GDEs

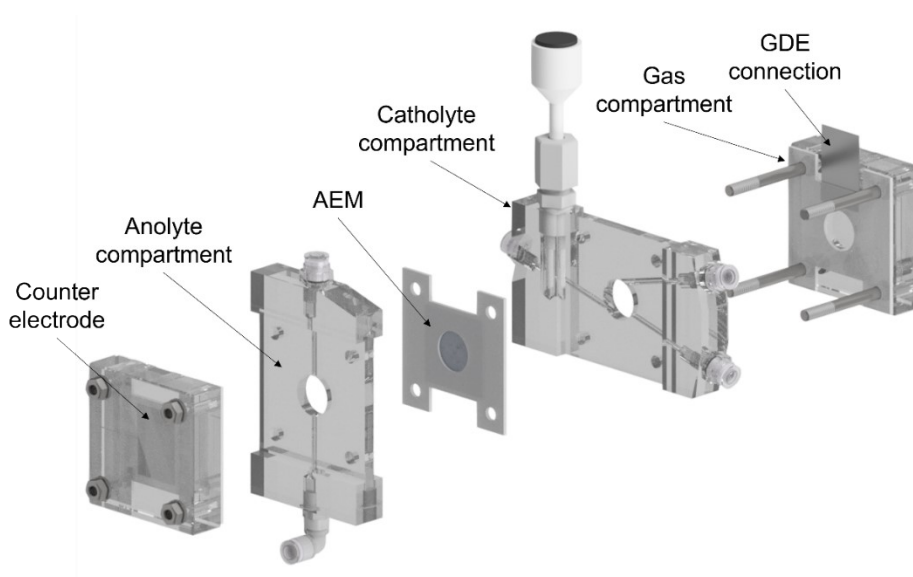


Figure 2: In-house built electrochemical flow cell for CO_2RR operation.

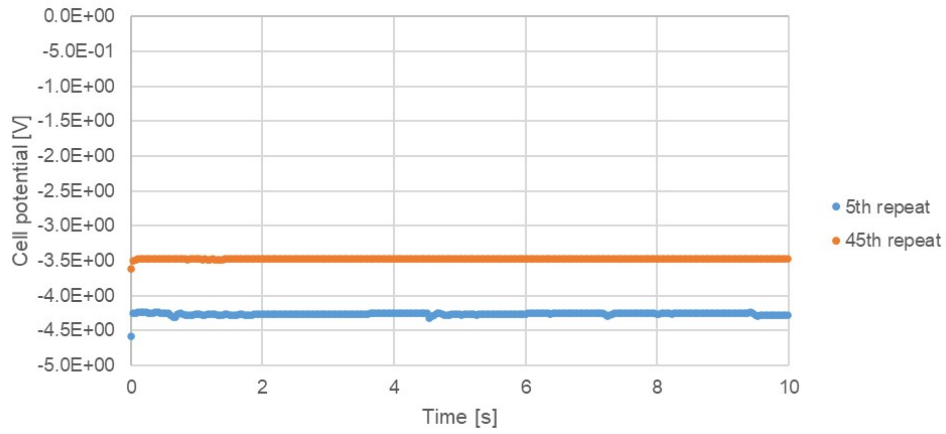


Figure 3: Cell potential during the fifth and the forty-fifth pulsating run.

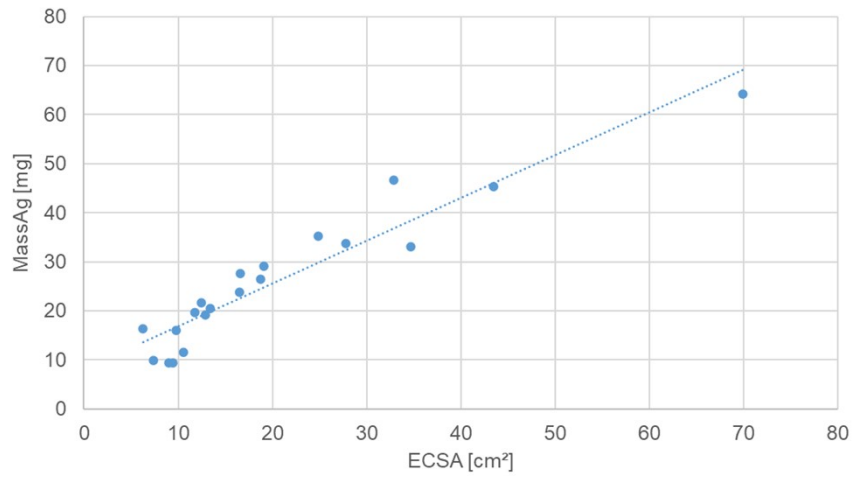


Figure 4: Correlation between the deposited Ag mass and the electrochemical surface area (ECSA) to establish a correlation factor.

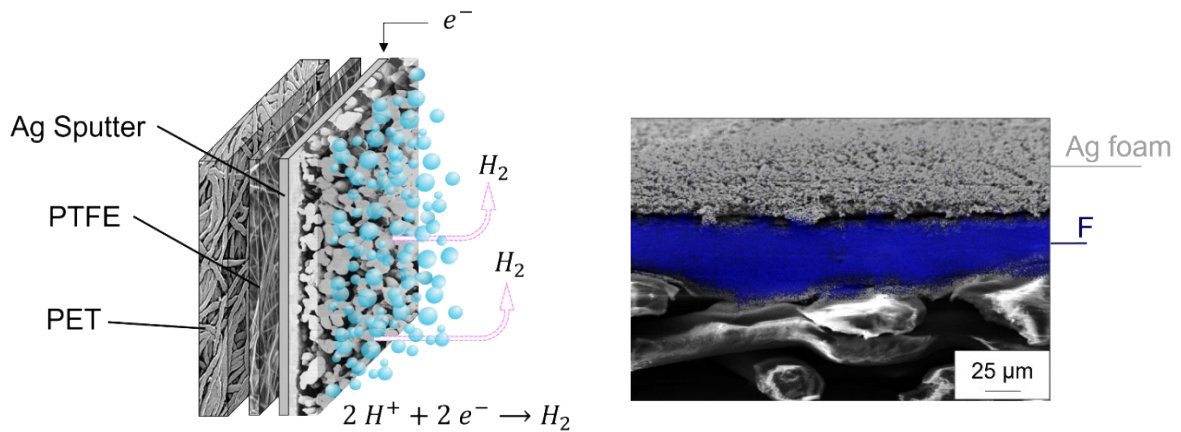


Figure 5: Graphical representation of the Dynamic Hydrogen Bubble Templatation process and the corresponding HER at the electrode surface (left) and SEM image of the resulting Ag foam on top of the polymer substrate (right).

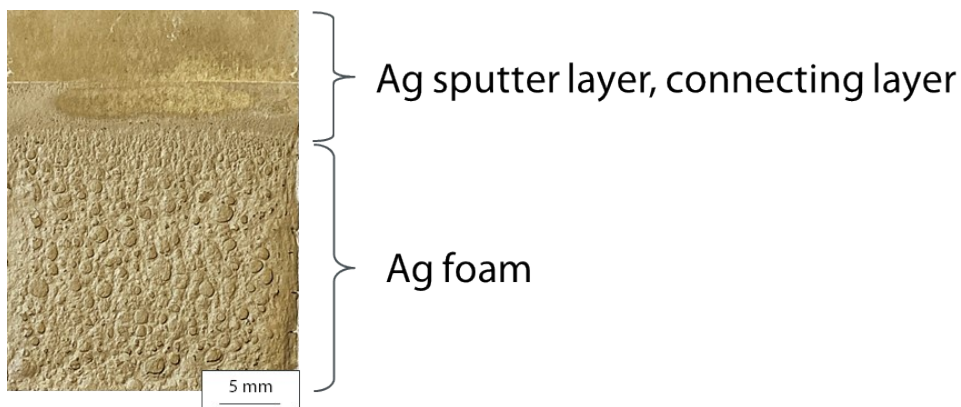


Figure 6: Image of a DHBT foam GDE.

Table 1: Values generated by physisorption measurements and capillary flow porometry for each sample.

Parameter	Unit	PET-PTFE	Ag-Sputter	DHBT Foam	Ionomer-infiltrated
BET	m ² g ⁻¹	0.69	0.85	0.88	0.35
Maximum Pore Size	μm	0.8974	0.3886	0.3925	0.4244
Mean Pore Size	μm	0.1492	0.1581	0.2426	0.2403
Minimum Pore Size	μm	0.1004	0.1145	0.2297	0.2045
Bubble Point Pressure	bar	0.7132	1.647	1.6307	1.5078
BubblePoint Flow Rate	Lm ⁻¹	0.1398	0.4013	0.3052	0.1054
Pore Volume	cm ³ g ⁻¹	34.49	37.57	37.72	20.76
Sample Thickness	μm	189	200	280	294
Sample Weight	g	0.0268	0.0268	0.04647	0.05116

Analysis before and after long term CO₂RR operation

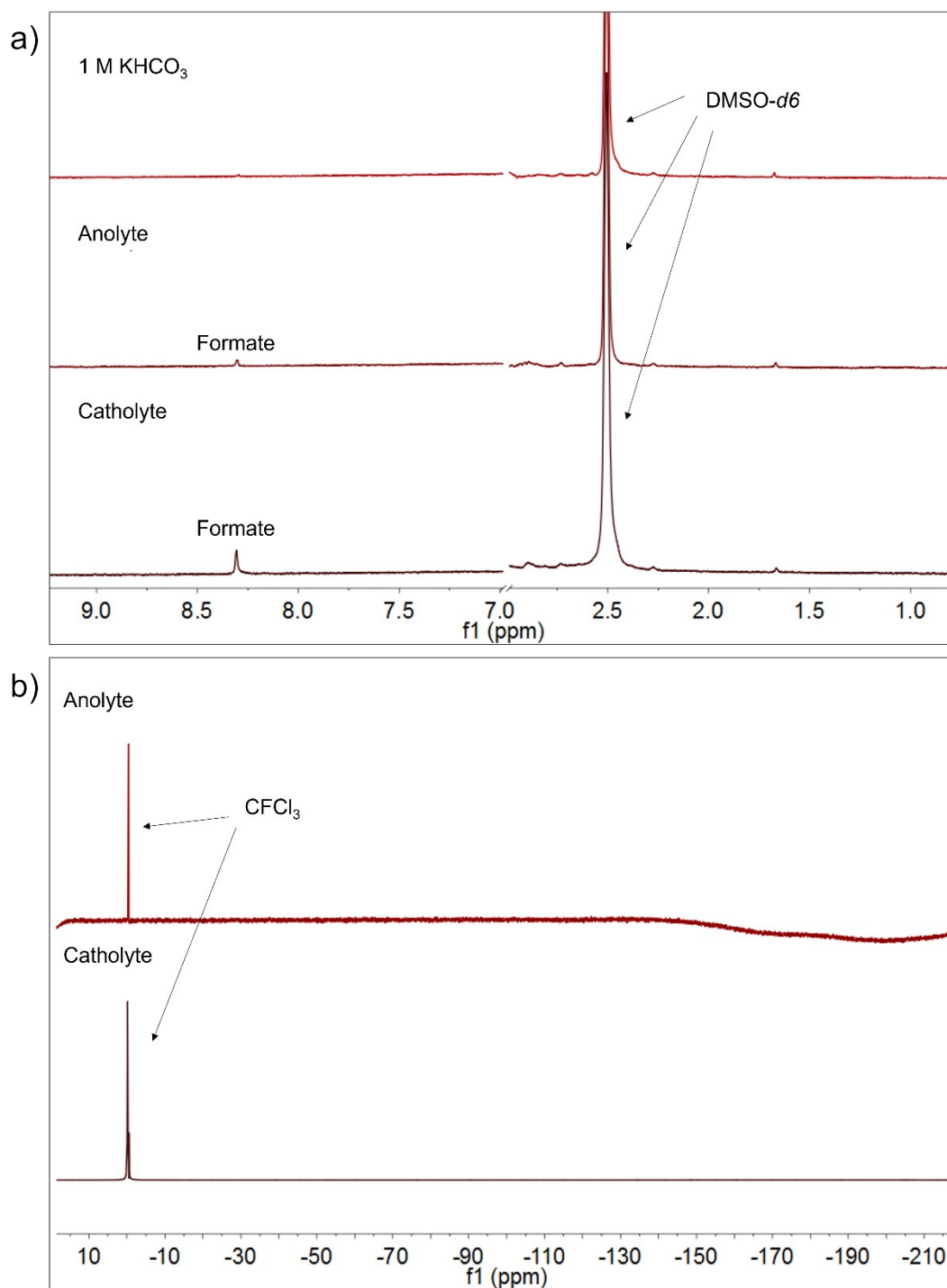


Figure 7: ¹H NMR spectra of the electrolytes (in DMSO-*d*₆) compartments and ¹⁹F NMR spectra of the electrolytes (in DMSO-*d*₆) after the long term stability test of the DHBT-GDE.

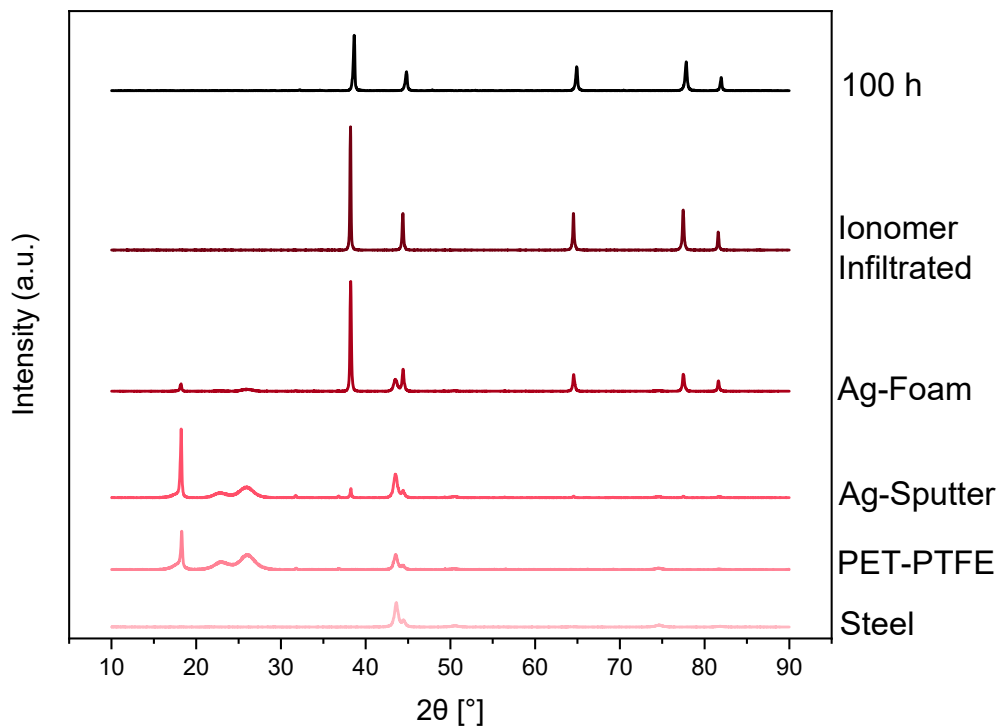


Figure 8: XRD pattern of the reference steel plate, PTFE-PET substrate, the Ag sputter layer, the Ag DHBT foam, the ionomer infiltrated GDE and the tested DHBT GDE after 100 h of CO₂RR operation.

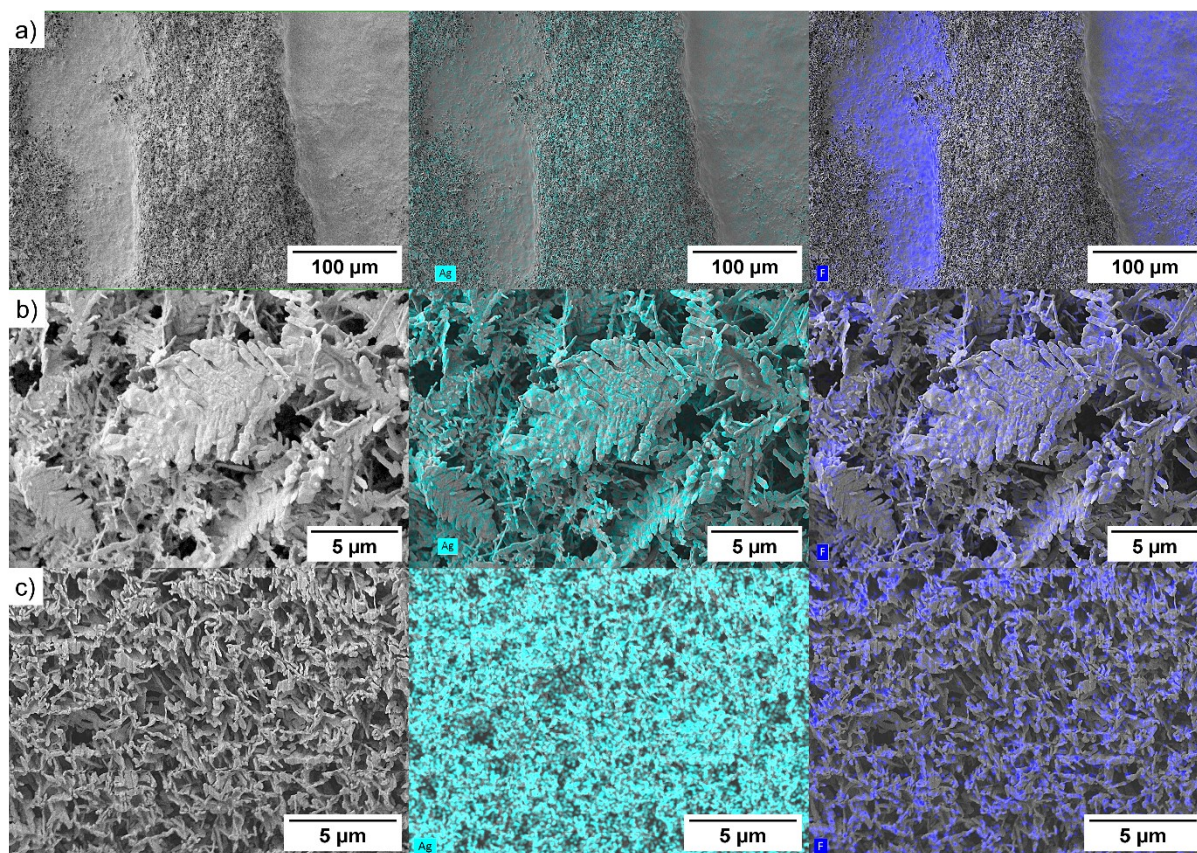


Figure 9: SEM images including EDS analysis of the Ag and F distribution on a pristine perfluorinated GDE. (a) Top down view, (b) zoomed-in view of the surface and (c) high resolution view of the nano-porous foam walls.

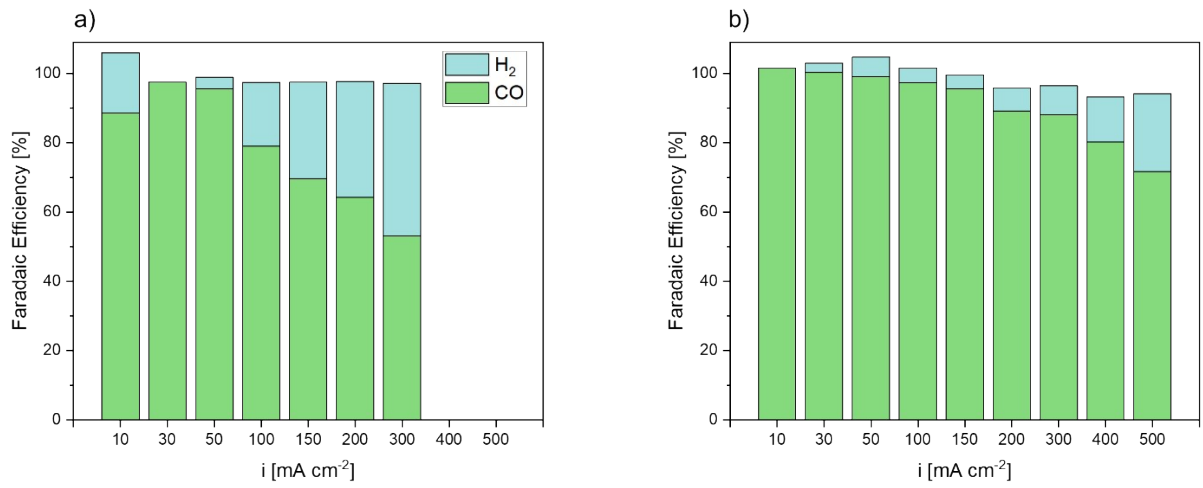


Figure 10: Faradaic efficiencies of CO and H₂ after galvanostatic operation at current densities up to 500 mA cm^{-2} . (a) CO₂RR results of a commercial Covestro GDE and (b) CO₂RR results of the Ag DHBT GDE.

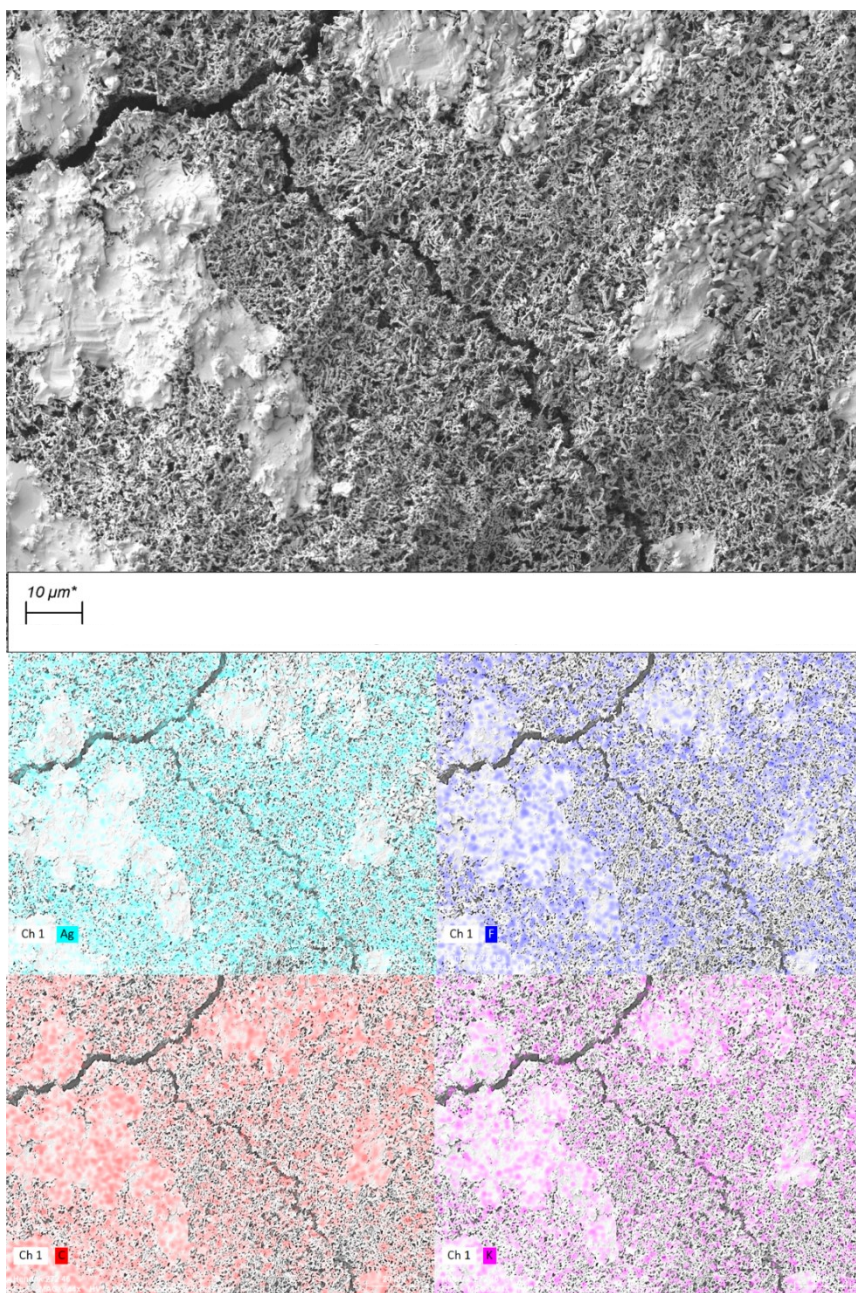


Figure 11: Top view SEM images (a) and EDS mapping analysis of Ag, F, C and K (b) of the Ag DHBT electrode after long-term CO₂RR operation at 200 mAcm⁻² for 100 h.

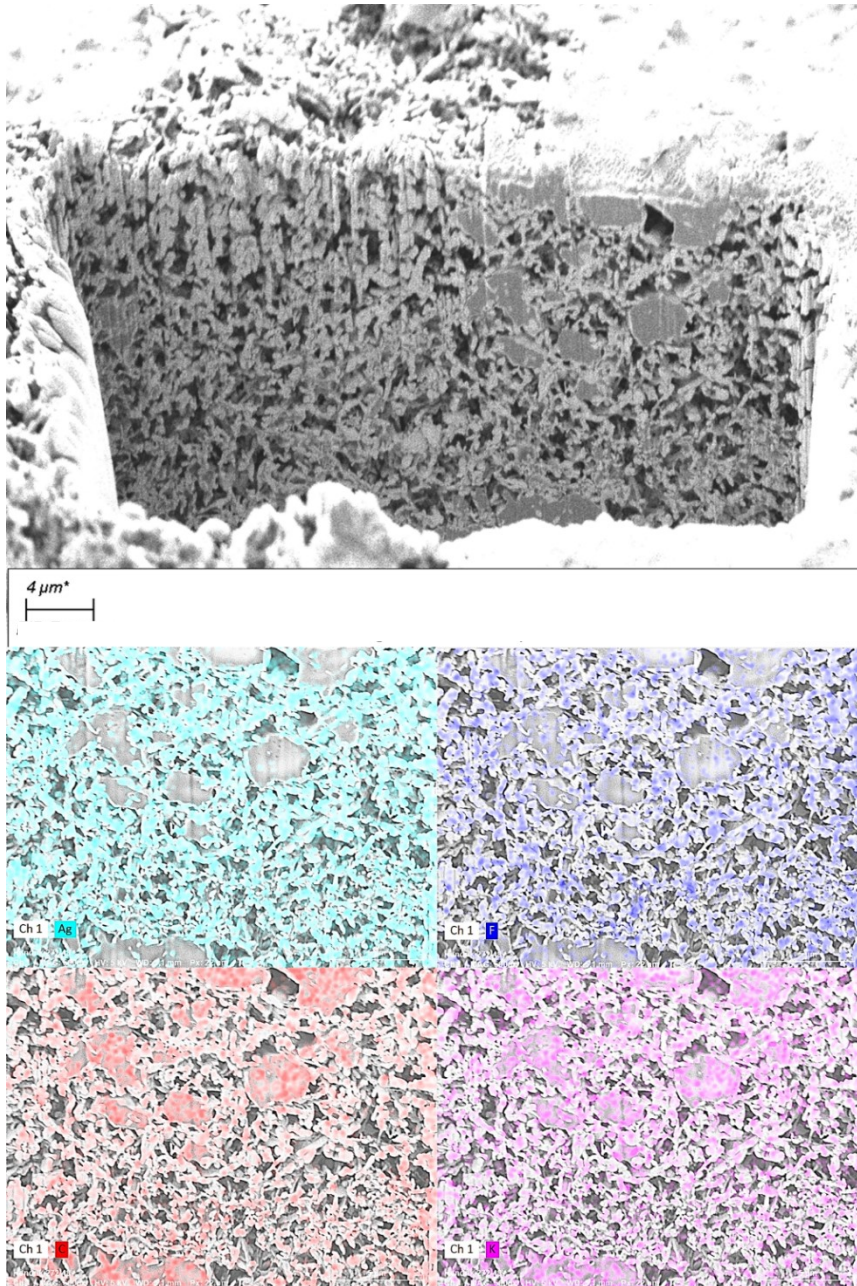


Figure 12: FIB cut view SEM images (a) and EDS mapping analysis of Ag, F, C and K (b) of the Ag DHBT electrode after long-term CO₂RR operation at 200 mAcm⁻² for 100 h.

Proposed reaction mechanism of the combined proton and electron donation step and the following splitting reaction based on work by Rosen et al.¹.

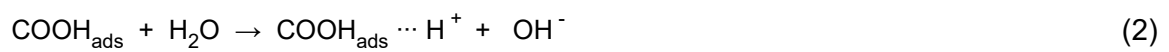


Table 2: Summary of CO₂RR long term performances for Ag electrodes in neutral and basic media.

Catalyst	Electrolytes	Current Density [mA/cm²]	Faradaic Efficiency [%]	Stability [h]	Reference
Ag/PFSA	1 M KHCO ₃	200	> 95	100	This work
Ag/PFSA	1 M KHCO ₃	500	> 75	1	This work
C/Ag/PTFE	1 M KHCO ₃	160	> 90	100	Dinh et al. ²
C/Ag/PTFE	1M KOH	150	> 90	100	Dinh et al. ²
Ag + Ionomer	1 M KHCO ₃	250	> 60	n. a.	García de Arquer et al. ³
Ag + Ionomer	1 M KHCO ₃	320	> 55	n. a.	García de Arquer et al. ³
Ag	2 M KHCO ₃	27	96	15	Monti et al. ⁴
Ag	1 M KOH	365	99	n. a.	Monti et al. ⁴
Ag/PTFE	1 M KOH	300	84	10	Gabardo et al. ⁵
Ag	1 M KHCO ₃	100	97	41	Senocrate et al. ⁶
Ag	1 M KHCO ₃	200	> 90	n. a.	Sassenburg et al. ⁷

References

1. Rosen, J. et al. Mechanistic Insights into the Electrochemical Reduction of CO₂ to CO on Nanostructured Ag Surfaces. *ACS Catal.* **5**, 4293–4299; 10.1021/acscatal.5b00840 (2015).
2. Dinh, C.-T., García de Arquer, F. P., Sinton, D. & Sargent, E. H. High Rate, Selective, and Stable Electroreduction of CO₂ to CO in Basic and Neutral Media. *ACS Energy Lett.* **3**, 2835–2840; 10.1021/acseenergylett.8b01734 (2018).
3. García de Arquer, F. P. et al. CO₂ electrolysis to multicarbon products at activities greater than 1 A cm⁻². *Science (New York, N.Y.)* **367**, 661–666; 10.1126/science.aay4217 (2020).
4. Monti, N. B. D. et al. Facile Fabrication of Ag Electrodes for CO₂ -to-CO Conversion with Near-Unity Selectivity and High Mass Activity. *ACS Appl. Energy Mater.* **5**, 14779–14788; 10.1021/acsaem.2c02143 (2022).
5. Gabardo, C. M. et al. Combined high alkalinity and pressurization enable efficient CO₂ electroreduction to CO. *Energy Environ. Sci.* **11**, 2531–2539; 10.1039/C8EE01684D (2018).
6. Senocrate, A. et al. Importance of Substrate Pore Size and Wetting Behavior in Gas Diffusion Electrodes for CO₂ Reduction. *ACS Appl. Energy Mater.* **5**, 14504–14512; 10.1021/acsaem.2c03054 (2022).
7. Sassenburg, M. et al. Characterizing CO₂ Reduction Catalysts on Gas Diffusion Electrodes: Comparing Activity, Selectivity, and Stability of Transition Metal Catalysts. *ACS Appl. Energy Mater.* **5**, 5983–5994; 10.1021/acsaem.2c00160 (2022).